Lasers in Manufacturing Conference 2021

# Adjusting the surface roughness of WE43 components manufactured by laser-based powder bed fusion

Tjorben Griemsmann[a,*], Niclas Söhnholz[a], Christian Hoff[a], Jörg Hermsdorf[a], Stefan Kaierle[a]

[a]*Laser Zentrum Hannover e.V., Hollerithallee 8, 30419 Hannover, Germany*

**Abstract**

The outstanding characteristics of magnesium alloys make them promising materials for biomedical or lightweight construction applications, especially in combination with the advantages of laser-based powder bed fusion. While most research in this field focusses porosity and microstructural properties, the surface quality is left out. Because the surface is an important factor for corrosion and notch effects, this work addresses the adjustment of the surface roughness from parts made out of a WE43 alloy. Using design of experiments contour scan trials are carried out for vertical and down skin surfaces. As a result, the roughness of vertical surfaces is reduced from approximately 27.1 µm (Ra) and 172.2 µm (Rz) without contour scans to 13.4 µm and 109.8 µm with contour scans. The applicability of the contour parameters is approved by cross sections to investigate the porosity of the contour volume interface.

Keywords: Laser-based powder bed fusion; Magnesium; Surface roughness; Design of experiments

## 1. Introduction

Magnesium is with a density of 1.74 g/cm$^3$ the lightest metallic constructional material and offers a high specific strength (Altwicker et al., 2001). This characteristic makes it an interesting material for lightweight constructions in space and aircraft to save expensive weight, but also in automotive technologies to reduce fuel consumption (Mordike and Ebert, 2001; Friedrich and Mordike, 2006). Besides lightweight applications magnesium and its alloys are gaining interest in biomedical engineering. The main reasons are bone like

* Corresponding author. Tel.: +49-511-2788-340; fax: +49-511-2788-100.
E-mail address: t.griemsmann@lzh.de .

mechanical properties and the ability to dissolve in the human body, also called bioresorbability. Next to an application in the cardio vascular system, e.g. as a self-dissolving stent, it offers high opportunities for orthopedic implants (Sillekens and Bormann, 2012; Chen et al., 2019; Bian et al., 2018).
Both lightweight construction and biomedical engineering represent a high demand for individual and highly complex product designs in order to manufacture topology optimized parts or patient individual implants. One economic way to fabricate individual and complex parts is through additive manufacturing techniques like laser-based powder bed fusion with metals (PBF-LB/M) (Vilardell et al., 2019; Guo and Leu, 2013; Paletti et al., 2020). For the process of PBF-LB a CAD model is sliced virtually with a specific thickness. To manufacture one layer, metal powder is applied with the layer thickness over the previous layer or build platform and selectively melted using a laser beam. The process iterates until the last slice is finished (Harun et al., 2019; Yap et al., 2015). Several research groups are investigating the PBF-LB/M process for magnesium alloys on a fundamental basis. Most of the research addresses achieving low porosities and characterizing mechanical properties. The most promising magnesium alloys for PBF-LB/M processing are the ones alloyed with aluminum and zinc (Wei et al., 2014; He et al., 2017; Pawlak et al., 2017; Liu et al., 2019) or with yttrium and rare earth (RE) elements (Gangireddy et al., 2019; Jauer, 2018; Gieseke et al., 2016; Abel et al., 2020) which show porosities lower than 1 % in the manufactured specimens. However, investigations regarding the surface roughness of the as build part are quite rare but important since the surface area influences the corrosion behavior. In this study contour scan trials are carried out for vertical and down skin surfaces using design of experiments (DoE) techniques to improve the surface quality of the as build parts.

## 2. Materials and methods

The powder used for the investigations is a gas atomized WE43 powder (Carpenter-Technology, formerly LPW-Technology) of the sieve fraction 20 µm to 63 µm. The dynamic image analysis revealed a D10 of 13.5 µm (10 % of all particles have a diameter below 13.5 µm), D50 of 31.4 µm and D90 of 58.5 µm. An overview of the particle shapes is given through the scanning electron microscopy (SEM) image in figure 1, using a Quanta 400 FEG (FEI Thermo Fisher Scientific). The sample shows that most of the particles have a spherical shape, but there are also some elonged and agglomerated particles. The chemical analysis of the powder, provided by the manucfacturer, is given in table 1.

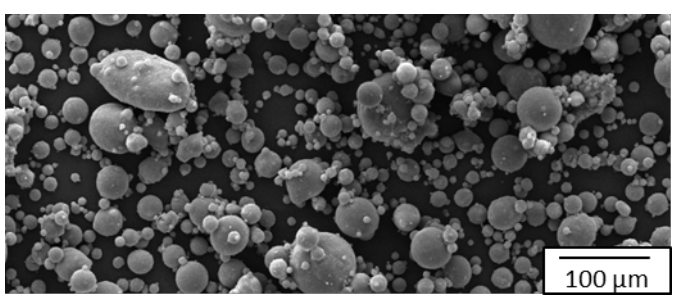


Fig. 1. SEM image of the used WE43 powder; most particles are spherical but also some agglomerations and deformed particles are found

Table 1. Chemical analysis of the used WE43 powder provided by the manufacturer

| Element | Magnesium | Copper | Iron | Manganese | Nickel | Silicon | Yttrium | Zinc | Zirconium | RE |
|---|---|---|---|---|---|---|---|---|---|---|
| Weight % | Bal. | 0.01 | <0.01 | 0.05 | 0.001 | <0.01 | 3.9 | 0.1 | 0.5 | 3.9 |

All PBF-LB/M processes are carried out using a SLM125$^{HL}$ (SLM Solutions Group AG) system with an ytterbium fiber laser in continuous wave mode. The laser emits at 1070 nm wavelength and has a maximum power output of 100 W. The optical path of the system includes a galvanometric scanner and an f-theta lens, which results in a focus diameter of 70 µm on the working plane. The maximum build space is 125 mm x 125 mm x 100 mm (w x l x h) and the residual oxygen content is lowered beneath 0.1 % using argon as an inert gas. The PBF-LB/M process data preparation, like placement of the specimen and specifying the PBF-LB/M process parameters, is carried out using AutoFab (Marcam Engineering, now Materialise GmbH).

### *2.1. Experimental methods and analysis*

In this study all investigations are done using the test specimen shown in figure 2. It has a square base with an edge length of 5 mm and is 5 mm high. There is a rectangular recess in the middle of the base plate and a side surface with a variable down skin angle α. The volume of each specimen is built with the exact same PBF-LB/M process parameters, because this study is only about the contour scans and not the volume itself. The process parameters used for the volume are a laser power P of 80 W, a scanning speed v of 450 mm/s, a hatch spacing h of 45 µm and a layer thickness t of 20 µm, based on previous investigations (Abel et al., 2020). Bidirectional unconnected stripes with a rotation of 60° per layer are used as hatching pattern as illustrated in

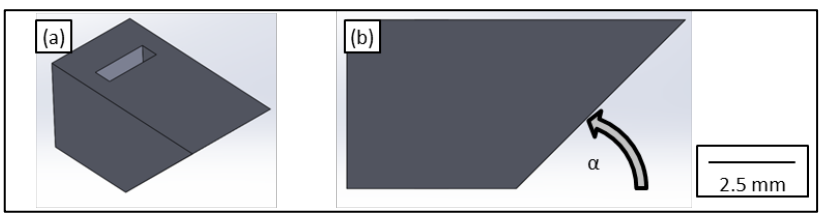


Fig. 2. (a) Isometric view of the test specimen; (b) side view with down skin angle α

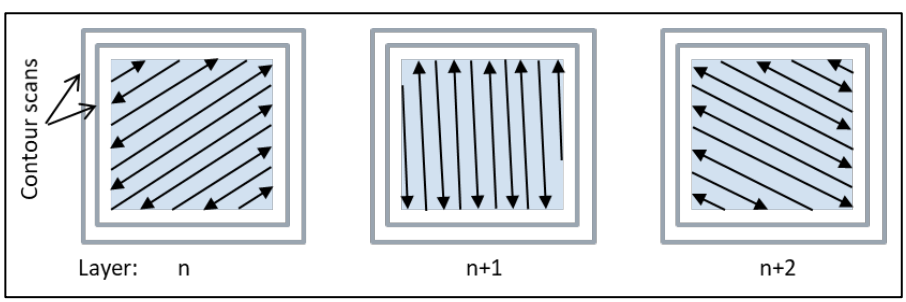


Fig. 3. Schematic illustration of the scanning path for three consecutive layers; each layer is rotated about 60°

figure 3.

The surface roughness is measured on the vertical walls or on the down skin surface, depending on the investigated feature. The roughness measurements are taken using a V-KX 1000 (Keyence) laser scanning microscope to determine the arithmetic mean roughness Ra and the average roughness Rz. On each sample 30 measurements are taken with a length of 2.7 mm. The mean and standard deviation is calculated for each sample. In order to examine any imperfections, such as pores in the interface of the contour and the volume of the sample, cross sections are made by embedding the sample in epoxy resin and afterwards grinding and polishing. The polished samples are examined by vision using the laser scanning microscope again. Eleven

samples of the test specimen are manufactured without contour scans in order to create a benchmark with which the results of the trials for the vertical and down skin surfaces can be compared.

### *2.2. Experimental design for vertical surfaces*

In a first step a parameter screening for the contour scans is carried out to achieve a general significance overview of the different process parameters. The examined PBF-LB/M process parameters are laser power P, scanning speed v, contour distance d, number of contour paths and the order of the contour paths (in to out/out to in). The distance from one contour to another is kept constant. Using the DoE approach *definitive screening design* 18 parameter combinations are generated from the process parameter values given in table 2 column 2. All examined parameter combinations are shown in table 3 in the appendix. The evaluation of the significance from the process parameters to the surface roughness is carried out using the statistics software JMP (SAS Institute).

Based on the results of the screening the main test run is designed using a *central composite design*. The used values for the process parameters are shown in table 2 column 3 (all combinations in table 4 in the appendix). The amount of different process parameters is reduced and more steps for the remaining laser power and contour distance are added, while the values are shifted to probably more appropriate settings. 18 different process parameter combinations are derived and samples manufactured three times with each combination to involve statistics. The results of the surface roughness measurements are used to fit a mathematical regression to predict the surface roughness as a function of the process parameters. Based on the regression an additional run is examined for further optimization. The values for the process parameters of the optimization run are given in table 2 column 4 (all combinations in table 5 in the appendix). The values for laser power and contour distance are shifted to lower or higher values, respectively. Nine process parameter combinations are derived using again a *central composite design*. Each combination is manufactured three times.

Table 2. Values of process parameters for the three consecutive experiment designs to improve the vertical surface roughness

| Process parameter | Values for screening run | Values for main run | Values for optimization run |
|---|---|---|---|
| Laser power P [W] | 50 / 75 / 100 | 20 / 35 / 50 / 65 / 80 | 12.5 / 20 / 27.5 / 35 / 42.5 |
| Scanning speed v [mm/s] | 300 / 475 / 600 | 475 | 475 |
| Contour distance d [µm] | 25 / 45 / 65 | 30 / 45 / 60 / 75 / 90 | 60 / 75 / 90 / 105 / 120 |
| Number of contour paths | 1 / 2 | 1 / 2 | 1 |
| Order of contour paths | In to out / out to in | Out to in | - |

To validate that a process parameter combination is not only resulting in a low surface roughness, but also in a dense contour volume interface, cross sections are made and discussed.

### *2.3. Experiment design for down skin surfaces*

The examinations concerning the contour scans of down skin surfaces are carried out for the down skin angles α 20°, 40° and 60° and laser powers of 23 W, 27.5 W and 32 W. The scanning speed and contour distance is not taken into account because of low effects in pre trials. The surface roughness is measured in the same way as for the vertical walls.

## 3. Results and discussion

### *3.1. Surface roughness on vertical surfaces*

The measured roughness without a contour scan is 27.1 ± 5.9 µm (Ra) and 172.2 ± 32.7 µm (Rz). The screening run was carried out to determine the significant PBF-LB/M process parameters. The results for the measured roughness values are given in table 3 of the appendix. The statistical evaluation reveals that only the number of contours and the laser power have a highly significant (p-value < 0.05) influence on the vertical surface roughness. The regression of the Ra values is plotted in figure 4 for the laser power, scanning speed, contour distance, contour order and number of contours. It is obvious that the scanning speed has not a great influence on the surface roughness in the examined range, as the plot is nearly horizontal. The influence of the contour order is not significant because of the high standard deviation. Next to the two significant process parameters, laser power and number of contours, the contour distance is also chosen for the main run, because of the promising lower surface roughness for high values.

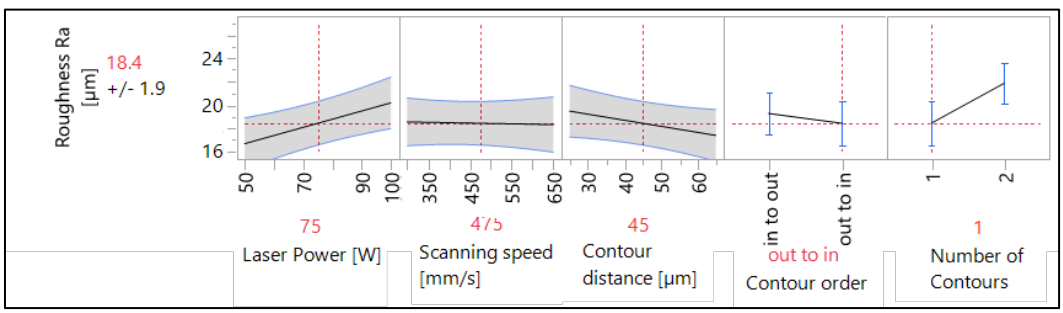


Fig. 4. Plot of the regression for the screening run; the scanning speed has nearly no effect on the surface roughness and one contour scan leads to smoother surfaces than two

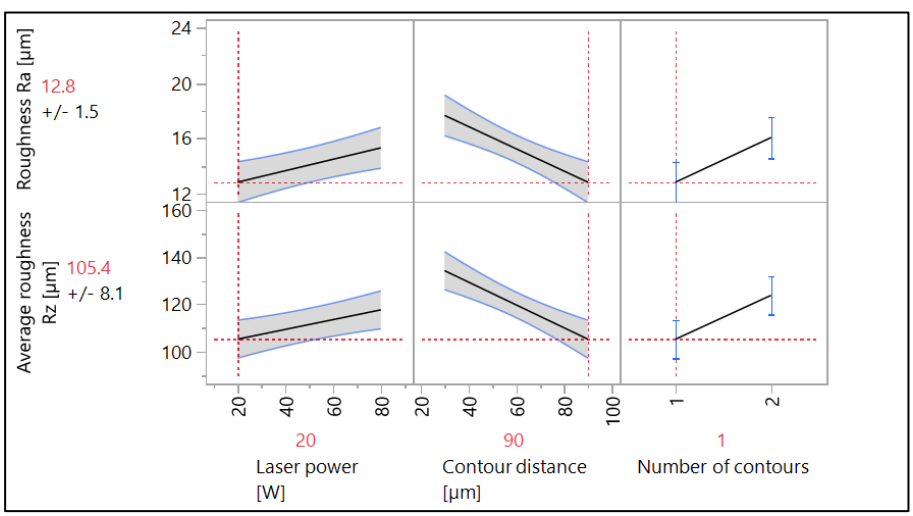


Fig. 5. Plot of predictions for the main run with the theoretically lowest roughness; the gradient for the contour distance switches to nearly zero if the number of contours is set to two

The results for the roughness measurements of all samples of the main run are provided in table 4 in the appendix. The lowest measured roughness is 13.2 ± 1.8 µm (Ra) and 106.9 ± 19.8 µm (Rz) for the process parameter combination P = 35 W, d = 75 µm and one contour scan. The statistical evaluation shows the highest significance for the interaction of the contour distance and the number of contours (p-value = 0.0007), the contour distance and laser power are with p-values of 0.0019 and 0.0022, respectively, also significant. Figure 5 shows plots for the prediction of the surface roughness. The values for both roughness sizes lower with decreasing laser power and with increasing contour distance. Two contour scans lead to higher roughness values and to nearly no influence of the contour distance. This is logical because between the outer most contour scan and the hatch of the volume is another contour scan with a constant distance to the outer most. So the contour distance does not influence the outer most contour scan. However, the surface roughness for trials with only one contour scan is lower than for two scans. For this reason the number of contours is fixed to one for the following trials. Because the plots of figure 5 show no minimum for the surface roughness it might be still possible to smooth the surfaces even more with an additional optimization run.

The results for the optimization run, with even lower laser powers and higher contour distances, are given in table 5 of the appendix. The lowest measured roughness is 11.6 ± 1.5 µm (Ra) and 107.0 ± 19.7 µm (Rz) for the process parameter combination of P = 20 W and d = 105 µm, which is only slightly lower as the best result for the main run. The results of the statistical examinations confirm a significant influence of the contour distance and the second order of the laser power (both p-value of 0.004). The plot of the regression in figure 6 (a) involves also the first order of the laser power (p-value of 0.068) and the second order of the contour distance (p-value of 0.12). Within this window of laser powers, a clear minimum can be found. This is explainable because the laser power does not supply enough intensity to melt the powder completely when the laser power falls below a certain value. Higher contour distances still lead to lower surface roughness but the trend seems to be asymptotic within the examined parameter window.

To determine how a high contour distance does affect the porosity in the contour volume interface, the results of the cross sections are discussed below and some representative examples are given in figure 7. For high contour distances (figure 7 (a)) a porous line can be found in the interface of the contour and the volume of the sample. This is because the melt pool size is not big enough to fully connect the contour to the volume. If the laser power is low (figure 7 (b)), no continuous contour is created. Figure 7 (c) shows a continuous and

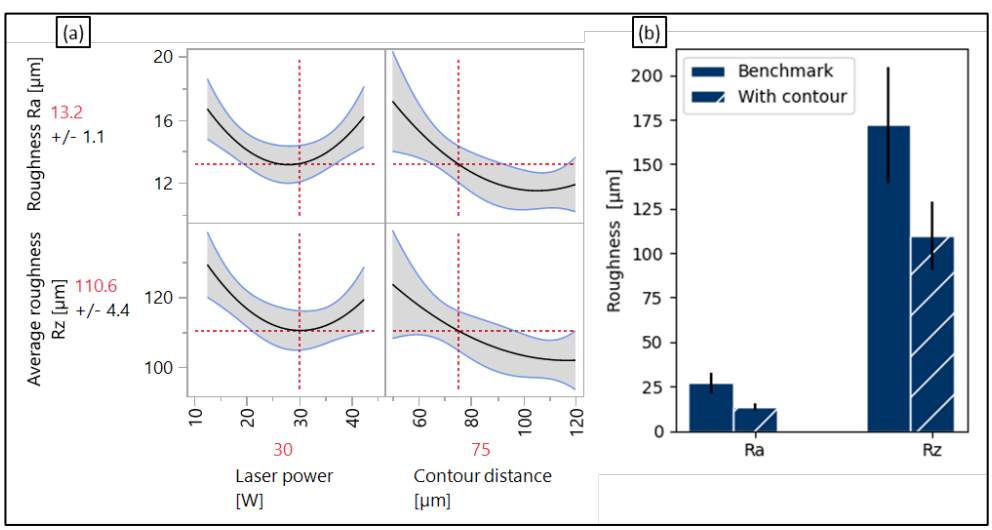


Fig. 6. (a) Plot of predictions for the optimization run; (b) comparison of the surface roughness with contour scans and without

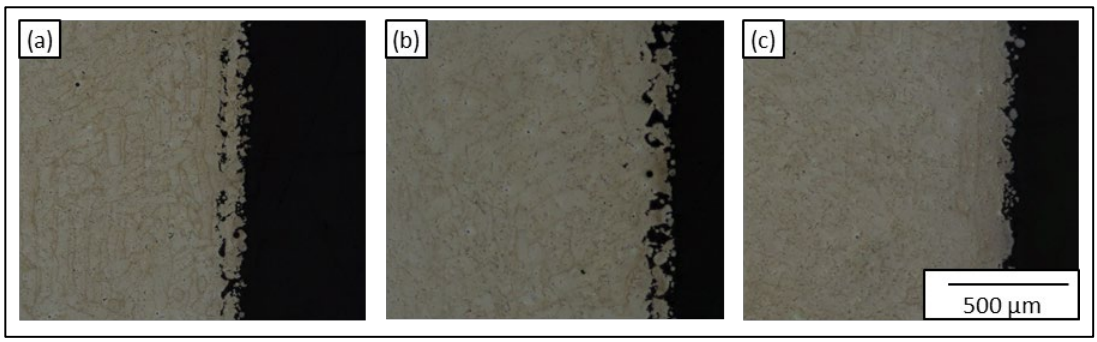


Fig. 7. Horizontal cross sections of specimens manufactured with: (a) P = 35 W, d = 105 µm, Ra = 12.7 µm; (b) P = 12.5 W, d = 90 µm, Ra = 14.5 µm; (c) P = 35 W, d = 75 µm, Ra = 12.4 µm

fully dense connection between the contour and the volume of the sample. To achieve this the contour distance should not be higher than 75 µm. From the predicted regression plot of figure 6 can be derived, that the theoretical minimal surface roughness with 75 µm contour distance is in the range around 30 W laser power with 13.2 ± 1.1 µm (Ra) and 110.6 ± 4.4 µm (Rz). The sample from figure 7 (c) is manufactured with a slightly different laser power of 35 W and the measured roughness is 13.4 ± 1.9 µm (Ra) and 109.8 ± 19.0 µm (Rz), which is close to the predicted roughness from the regression of figure 6. Figure 6 (b) shows a comparison of the achieved surface roughness with the roughness of the benchmark without a contour scan. Ra is reduced by approx. 50 % and Rz by approx. 37 %. The DoE approach, in combination with cross sections to ensure a proper contour volume interface, is therefore highly applicable to adjust or minimize the vertical surface roughness of WE43 components.

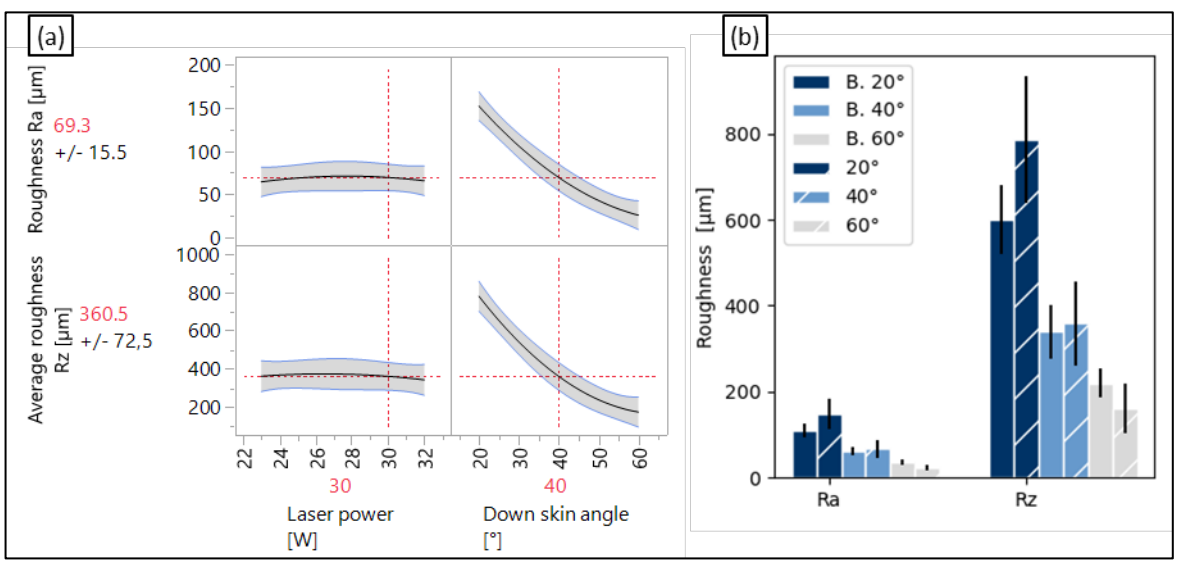


Fig. 8 (a). Regression plot for the surface roughness as a function of the laser power and down skin angle; the laser power has nearly no influence on the surface roughness while the roughness decreases with an increasing down skin angle; (b) the benchmark samples (B.) show lower surface roughness than the samples with contour scan, except for an down skin angle of 60°

### *3.2. Surface roughness on down skin surfaces*

The results of the measurements on down skin surfaces with angles of 20°, 40° and 60° are given in table 6 in the appendix. The range of laser power values was chosen considering the results for the vertical surfaces. In this range, there is no influence of the laser power on the surface roughness on down skin surfaces. On the other hand, the down skin angle itself has a high impact on the surface roughness as expected and shown in figure 8 (a). In figure 8 (b) the roughness of all samples with contour scan and the same down skin angle are averaged and compared to the benchmark result. With decreasing down skin angle there is a negative impact on the surface roughness. Only the samples with 60° down skin angle are showing a smoother surface using a contour scan, with 23.4 ± 7.9 µm (Ra) and 161.4 ± 58.2 µm (Rz), compared to 37.3 ± 6.2 µm (Ra) and 220 ± 32.9 µm (Rz) without a contour. One explanation could be through the low vaporization point of magnesium. With lower down skin angles the contour is mostly scanned directly over unmold powder and therefore higher temperatures can occur as for the hatch pattern, where the melt pool is better connected to the volume of the sample. In addition, the contour is scanned before the hatch pattern, which results in less volume to dissipate the heat.

## 4. Conclusion

In this work the surface roughness of WE43 processed by PBF-LB/M was adjusted and optimized using contour scans and DoE techniques. The surface roughness was lowered by 50 % to 13.4 ± 1.9 µm (Ra) and by 37 % to 109.8 ± 19.0 µm (Rz) with a dense interface from the volume to the contour. The laser power and the distance from the contour to the volume of the sample had the strongest effect on the surface roughness.

The down skin surface was slightly smoothed for higher down skin angles, but for lower angles the contour scan led to higher roughness values. The laser power had no influence on the down skin surface roughness. This is probably because of the small range of examined laser power values and the high mean variation of the results. Further investigations should involve different scanning strategies for down skin surfaces and the directly surrounding volume hatch.

## References

Abel, Wessarges, Julmi, Hoff, Hermsdorf, Klose, Maier, Kaierle, and Overmeyer. 2020. Laser Powder Bed Fusion of WE43 in Hydrogen-Argon-Gas Atmosphere. Procedia CIRP 94: 21–24. https://doi.org/10.1016/j.procir.2020.09.005.

Altwicker, Bauer, Beck, Bohner, Buchmann, Fiedler, Gossrau, et al., eds. 2001. *Magnesium Und Seine Legierungen*. Berlin, Heidelberg: Springer Berlin Heidelberg. https://doi.org/10.1007/978-3-642-56708-7.

Bian, Deng, Li, Chu, Liu, Li, Cai, et al. 2018. In Vitro and in Vivo Studies on Biomedical Magnesium Low-Alloying with Elements Gadolinium and Zinc for Orthopedic Implant Applications. ACS Applied Materials & Interfaces 10 (5): 4394–4408. https://doi.org/10.1021/acsami.7b15498.

Chen, Dou, Yu, and Chen. 2019. Degradable Magnesium-Based Alloys for Biomedical Applications: The Role of Critical Alloying Elements. Journal of Biomaterials Applications 33 (10): 1348–72. https://doi.org/10.1177/0885328219834656.

Friedrich, and Mordike, eds. 2006. *Magnesium Technology*. Berlin/Heidelberg: Springer-Verlag. https://doi.org/10.1007/3-540-30812-1.

Gangireddy, Gwalani, Liu, Faierson, and Mishra. 2019. Microstructure and Mechanical Behavior of an Additive Manufactured (AM) WE43-Mg Alloy. Additive Manufacturing 26 (March): 53–64. https://doi.org/10.1016/j.addma.2018.12.015.

Gieseke, Kiesow, Wessarges, Nölke, Kaierle, Maier, Matena, Kampmann, Escobar, and Nolte. 2016. Challenges of Processing Magnesium and Magnesium Alloys by Selective Laser Melting. In European Congress and Exhibition on Powder Metallurgy. European PM Conference Proceedings, 1–6. The European Powder Metallurgy Association.

Guo, and Leu. 2013. Additive Manufacturing: Technology, Applications and Research Needs. Frontiers of Mechanical Engineering 8 (3): 215–43. https://doi.org/10.1007/s11465-013-0248-8.

Harun, Kadirgama, Samykano, Ramasamy, Ahmad, and Moradi. 2019. Mechanical Behavior of Selective Laser Melting-Produced Metallic Biomaterials. In Mechanical Behaviour of Biomaterials, 101–16. Elsevier. https://doi.org/10.1016/B978-0-08-102174-3.00005-X.

He, Bin, Wu, Gao, Feng, Yang, Liu, et al. 2017. Microstructure Evolution and Biodegradation Behavior of Laser Rapid Solidified Mg–Al–Zn Alloy. Metals 7 (3): 105. https://doi.org/10.3390/met7030105.

Jauer. 2018. Laser Powder Bed Fusion von Magnesiumlegierungen. Ergebnisse Aus Der Lasertechnik. Apprimus Wissenschaftsver.

Liu, Yang, Shi, Li, Duan, Guo, and Guo. 2019. Influence of Laser Process Parameters on the Densification, Microstructure, and Mechanical Properties of a Selective Laser Melted AZ61 Magnesium Alloy. Journal of Alloys and Compounds 808 (November): 151160. https://doi.org/10.1016/j.jallcom.2019.06.261.

Mordike, and Ebert. 2001. Magnesium. Materials Science and Engineering: A 302 (1): 37–45. https://doi.org/10.1016/S0921-5093(00)01351-4.

Paletti, van den Brink, Bruins, Ven, and Bosman. 2020. Additive Manufacturing Design in Aerospace: Topology Optimization and Virtual Manufacturing.

Pawlak, Rosienkiewicz, and Chlebus. 2017. Design of Experiments Approach in AZ31 Powder Selective Laser Melting Process Optimization. Archives of Civil and Mechanical Engineering 17 (1): 9–18. https://doi.org/10.1016/j.acme.2016.07.007.

Sillekens, and Bormann. 2012. Biomedical Applications of Magnesium Alloys. Advances in Wrought Magnesium Alloys, 427–54. https://doi.org/10.1533/9780857093844.3.427.

Vilardell, Takezawa, du Plessis, Takata, Krakhmalev, Kobashi, Yadroitsava, and Yadroitsev. 2019. Topology Optimization and Characterization of Ti6Al4V ELI Cellular Lattice Structures by Laser Powder Bed Fusion for Biomedical Applications. Materials Science and Engineering A 766 (October): 138330. https://doi.org/10.1016/j.msea.2019.138330.

Wei, Gao, Wang, and Zeng. 2014. Effect of Energy Input on Formability, Microstructure and Mechanical Properties of Selective Laser Melted AZ91D Magnesium Alloy. Materials Science and Engineering A 611 (August): 212–22. https://doi.org/10.1016/j.msea.2014.05.092.

Yap, Chua, Dong, Liu, Zhang, Loh, and Sing. 2015. Review of Selective Laser Melting: Materials and Applications. Applied Physics Reviews 2 (4): 041101. https://doi.org/10.1063/1.4935926.

## Appendix A. Process parameter combinations and roughness results

Table 3. Process parameter combinations and results for the vertical surfaces screening run

| # | Laser power [W] | Scanning speed [µm] | Contour distance [µm] | Number of contours | Order of contours | Arithmetic mean roughness Ra [µm] | Average Roughness RZ [µm] |
|---|---|---|---|---|---|---|---|
| 1 | 100 | 650 | 25 | 1 | Out to in | 23.7 ± 3.3 | 158.1 ± 23.9 |
| 2 | 100 | 300 | 45 | 2 | Out to in | 25.5 ± 3.7 | 169.3 ± 22.6 |
| 3 | 50 | 475 | 25 | 2 | In to out | 24.8 ± 3.0 | 171.1 ± 26.5 |
| 4 | 100 | 300 | 25 | 2 | Out to in | 24.0 ± 3.9 | 170.6 ± 23.8 |
| 5 | 75 | 300 | 25 | 1 | In to out | 21.1 ± 3.6 | 166.6 ± 30.8 |
| 6 | 75 | 475 | 45 | 1 | In to out | 17.4 ± 1.6 | 133.9 ± 17.6 |
| 7 | 100 | 650 | 65 | 2 | In to out | 26.0 ± 3.9 | 184.5 ± 25.8 |
| 8 | 75 | 650 | 65 | 2 | Out to in | 20.1 ± 3.2 | 153.2 ± 23.6 |
| 9 | 50 | 650 | 25 | 2 | Out to in | 19.4 ± 2.4 | 146.2 ± 21.7 |
| 10 | 100 | 475 | 65 | 1 | Out to in | 19.2 ± 2.6 | 148.1 ± 28.8 |
| 11 | 50 | 300 | 25 | 1 | Out to in | 17.7 ± 2.6 | 146.6 ± 24.0 |
| 12 | 100 | 650 | 25 | 2 | In to out | 23.6 ± 3.2 | 168.2 ± 21.5 |
| 13 | 75 | 475 | 45 | 2 | Out to in | 19.3 ± 2.9 | 143.8 ± 22.8 |
| 14 | 100 | 300 | 65 | 1 | In to out | 17.8 ± 2.7 | 140.8 ± 27.2 |

| | | | | | | | |
|---|---|---|---|---|---|---|---|
| 15 | 50 | 300 | 65 | 2 | In to out | 20.2 ± 3.5 | 158.1 ± 31.9 |
| 16 | 50 | 300 | 65 | 1 | Out to in | 17.0 ± 3.2 | 141.8 ± 26.9 |
| 17 | 50 | 650 | 45 | 1 | In to out | 16.5 ± 2.7 | 135.3 ± 30.3 |
| 18 | 50 | 650 | 65 | 1 | In to out | 16.7 ± 2.4 | 124.9 ± 23.0 |

Table 4. Process parameter combinations and results for the vertical surfaces main run

| # | Laser power [W] | Contour distance [µm] | Number of contours | Arithmetic mean roughness Ra [µm] | Average Roughness RZ [µm] |
|---|---|---|---|---|---|
| 1 | 35 | 75 | 2 | 15.4 ± 2.0 | 121.2 ± 21.5 |
| 2 | 65 | 45 | 2 | 17.6 ± 2.5 | 135.5 ± 22.0 |
| 3 | 50 | 60 | 1 | 16.0 ± 2.4 | 129.4 ± 25.3 |
| 4 | 65 | 75 | 1 | 15.7 ± 2.1 | 117.4 ± 18.8 |
| 5 | 80 | 60 | 1 | 18.8 ± 2.7 | 135.6 ± 22.0 |
| 6 | 65 | 45 | 1 | 16.7 ± 2.5 | 133.4 ± 24.3 |
| 7 | 50 | 90 | 2 | 17.1 ± 2.7 | 133.7 ± 26.2 |
| 8 | 20 | 60 | 2 | 16.1 ± 3.5 | 124.1 ± 26.3 |
| 9 | 35 | 45 | 1 | 15.5 ± 2.3 | 124.7 ± 24.0 |
| 10 | 35 | 75 | 1 | 13.2 ± 1.8 | 106.9 ± 19.8 |
| 11 | 50 | 60 | 2 | 17.4 ± 3.0 | 132.0 ± 21.1 |
| 12 | 50 | 30 | 2 | 16.6 ± 2.5 | 128.2 ± 25.2 |
| 13 | 20 | 60 | 1 | 17.3 ± 4.7 | 123.6 ± 25.3 |
| 14 | 65 | 75 | 2 | 19.2 ± 2.9 | 134.2 ± 20.3 |
| 15 | 35 | 45 | 2 | 16.4 ± 2.5 | 126.5 ± 23.3 |
| 16 | 80 | 60 | 2 | 17.6 ± 2.8 | 128.6 ± 20.2 |
| 17 | 50 | 30 | 1 | 20.5 ± 2.7 | 144.8 ± 24.8 |
| 18 | 50 | 90 | 1 | 14.9 ± 2.2 | 118.4 ± 20.2 |

Table 5. Process parameter combinations and results for the vertical surfaces optimization run

| # | Laser power [W] | Contour distance [µm] | Arithmetic mean roughness Ra [µm] | Average Roughness RZ [µm] |
|---|---|---|---|---|
| 1 | 35.0 | 105 | 12.7 ± 1.6 | 102.8 ± 18.3 |
| 2 | 27.5 | 90 | 11.9 ± 1.4 | 107.4 ± 21.3 |
| 3 | 42.5 | 90 | 14.9 ± 2.3 | 115.8 ± 23.1 |
| 4 | 35.0 | 75 | 13.4 ± 1.9 | 109.8 ± 19.0 |
| 5 | 20.0 | 75 | 14.8 ± 2.9 | 119.6 ± 20.7 |
| 6 | 27.5 | 60 | 15.2 ± 2.6 | 117.5 ± 21.5 |
| 7 | 12.5 | 90 | 15.5 ± 2.5 | 123.6 ± 23.4 |
| 8 | 27.5 | 120 | 12.0 ± 1.4 | 103.9 ± 20.6 |
| 9 | 20.0 | 105 | 11.6 ± 1.5 | 107.0 ± 19.7 |

Table 6. Process parameter combinations and results for down skin surfaces

| # | Laser power [W] | Down skin angle [°] | Arithmetic mean roughness Ra [µm] | Average Roughness RZ [µm] |
|---|---|---|---|---|
| 1 | 23.0 | 60 | 23.2 ± 5.4 | 153.1 ± 34.5 |
| 2 | 27.5 | 60 | 27.4 ± 10.6 | 192.8 ± 81.3 |
| 3 | 32.0 | 60 | 19.5 ± 3.7 | 138.3 ± 28.0 |
| 4 | 23.0 | 40 | 68.3 ± 17.1 | 361.8 ± 91.1 |
| 5 | 27.5 | 40 | 55.3 ± 9.2 | 302.6 ± 57.4 |
| 6 | 32.0 | 40 | 76.7 ± 23.9 | 411.3 ± 106.7 |
| 7 | 23.0 | 20 | 139.7 ± 25.5 | 800.5 ± 114.9 |
| 8 | 27.5 | 20 | 168.5 ± 36.2 | 852.2 ± 151.6 |
| 9 | 32.0 | 20 | 138.9 ± 34.1 | 708.0 ± 136.2 |